

Delta-alpha cross-frequency coupling for different brain regions

Dushko Lukarski,^{1,2} Spase Petkoski,³ Peng Ji,⁴ and Tomislav Stankovski^{1,5}

^{1)Faculty of Medicine, Ss. Cyril and Methodius University, 1000 Skopje, Macedonia.}

^{2)University Clinic for Radiotherapy and Oncology, 1000 Skopje, Macedonia.}

^{3)Aix Marseille Univ, INSERM, Inst Neurosci Syst (INS), 13005 Marseille, France}

^{4)Institute of Science and Technology for Brain-Inspired Intelligence, Fudan University, 200433 Shanghai, China}

^{5)Department of Physics, Lancaster University, LA1 4YB Lancaster, United Kingdom.}

(*Electronic mail: t.stankovski@ukim.edu.mk.)

(Dated: 28 September 2023)

Neural interactions occur on different levels and scales. It is of particular importance to understand how they are distributed among different neuroanatomical and physiological relevant brain regions. We investigated neural cross-frequency couplings between different brain regions according to the Desikan-Killiany brain parcellation. The adaptive dynamic Bayesian inference method was applied to EEG measurements of healthy resting subjects in order to reconstruct the coupling functions. It was found that even after averaging over all subjects, the mean coupling function showed a characteristic waveform, confirming the direct influence of the delta-phase on the alpha-phase dynamics in certain brain regions and that the shape of the coupling function changes for different regions. While the averaged coupling function within a region was of similar form, the region-averaged coupling function was averaged out, which implies that there is a common dependence within separate regions across the subjects. It was also found that for certain regions the influence of delta on alpha oscillations is more pronounced and that oscillations that influence other are more evenly distributed across brain regions than the influenced oscillations. When presenting the information on brain lobes, it was shown that the influence of delta emanating from the brain as a whole is greatest on the alpha oscillations of the cingulate frontal lobe, and at the same time the influence of delta from the cingulate parietal brain lobe is greatest on the alpha oscillations of the whole brain.

The delta-alpha cross-frequency coupling is proving to be a valuable descriptor in increasingly more brain states and domains. Here, by applying the adaptive dynamic Bayesian inference to EEG signals of subjects at rest we reconstructed the neural cross-frequency delta to alpha coupling functions that describe the interaction mechanisms of different regions of the brain. With this analysis framework we found a number of significant brain connections, as well as several characteristic differences between the brain regions.

I. INTRODUCTION

The interactions in the brain are fundamental to the human ability to perceive and interact with the world. The brain is a heavily connected dynamical network system¹, with interactions that are very complex and involve a vast network of neurons and synapses. Such complex system can mediate a vast number of functions, from a relatively static structure. Importantly, the brain can evolve with time, and different changes and transitions can occur^{2,3}. Because not all the neurons and network processes in the brain are active at all time, and because they can exhibit collective, clustered, and synchronized behaviour⁴⁻⁶, different types of changes, disruptions and transitions in the neural activity can occur^{7,8}.

Since the functions of the brain are highly dependent on its structure, and different functions are probably performed by different brain regions with different architecture, it is essential to identify the different regions of the brain in order to

better understand its functions. For that reason, a significant effort has been invested by the scientific community in the direction of parcellation of the brain, starting from the classic Brodmann map, through the widely used Desikan-Killiany atlas⁹, all the way to the recently published human Brainnetome atlas¹⁰ and Human Connectome Project (HCP) multi-modal parcellation¹¹ using *in vivo* MRI data.

The brain connectivity is crucial to understand how the neurons and the brain dynamics evolve. A particularly accessible and useful approach has been the study of neural cross-frequency coupling, usually extracted from an electroencephalograph (EEG) recording¹²⁻¹⁶. Neural cross-frequency coupling refers to the interaction between different frequencies of neural brainwave oscillations in the brain. Cross-frequency coupling occurs when the amplitude or phase of one frequency band of oscillations is modulated by another frequency band. Thus, there are different types of cross-frequency coupling, such as amplitude-amplitude coupling, phase-phase coupling, and amplitude-phase coupling.

Neural cross-frequency coupling can be studied between different combinations of brainwave oscillations. In this work, we will focus on the delta-to-alpha neural cross-frequency coupling. Namely, it is well known that delta and alpha brainwave oscillations play an important role in the brain dynamics¹⁷⁻²². For instance, there are differences in frequency and power during different sleep stages which appear in the separate delta and alpha brainwave dynamics²³⁻²⁶ and in their related delta-alpha effect^{27,28}. In another example, in a previous study about general anaesthesia²⁹ it was found that the delta-alpha coupling function is statistically significant and strong during anaesthesia. Similarly, previous works observe a prominent delta-alpha coupling in resting state^{15,30}, during

the orienting response³² and during sleep within the network physiology approach²⁰. A characteristic form of the delta-alpha coupling functions was also established²⁹⁻³¹. These works point out that the choice to investigate the delta-to-alpha coupling among the brain regions had a relevance for the present study of resting state.

To perform the analysis needed we used comprehensive set of methods. First, to observe the oscillatory content of the brainwave oscillations we used wavelet time-frequency analysis. Then, we used the fact that the delta and alpha brainwaves have pronounced oscillating dynamics in order to study the interactions through their reduced phase dynamics³³, thus observing phase-phase cross-frequency coupling. Here, we applied a method based on adaptive dynamical Bayesian inference for analysis of data to reconstruct a dynamical phase model describing the systems and their interactions³⁴⁻³⁶. The method of dynamical inference reconstructs effective connectivity^{1,37} and reveals the underlying dynamical mechanisms. Here, we reconstruct the phase *coupling functions* which describe how the interaction occurs and manifest, thus revealing a functional mechanism³⁸. The design of powerful methods and the explicit assessment of coupling functions have led to applications in different scientific fields including chemistry³⁹, climate⁴⁰, secure communications⁴¹, mechanics⁴², social sciences⁴³, and oscillatory interaction in physiology for cardiorespiratory interactions^{44,45}. Arguably, the greatest recent interest for coupling functions is coming from neuroscience⁴⁶, where works have encompassed the theory and inference of a diversity of neural phenomena, physical regions, and physiological conditions^{30,47-53}.

II. MATERIALS AND METHODS

A. Adaptive Dynamical Bayesian Inference

When investigating a complex dynamical oscillatory system, such as the oscillatory behaviour of the brain, one way to gain new insights is by modeling the system by using differential equations. Usually, by measuring some signals originating from the oscillatory time evolution of the system, one can infer the parameters of a model that describes the system under certain conditions. According to the phase reduction theory, in case when the interactions between the oscillators are sufficiently weak, the behaviour of the system can be approximated with its phase dynamics^{33,54,55}. If the phases of the system can be considered as monotonic change of the variables, the partial dynamical process of the node i as influenced by another node j can be represented with the system of differential equations:

$$\dot{\varphi}_{i,j} = \omega_i + q_{i,j}(\varphi_i, \varphi_j) + \xi_i, \quad (1)$$

where φ_i is the phase of the i -th oscillator, ω_i is its angular frequency parameter, $q_{i,j}$ is the coupling function which describes the influence of the j -th oscillator on the i -th oscillator, and ξ_i represents the noise. Usually, the noise is assumed as a white Gaussian noise given by $\xi_i(t)\xi_j(\tau) = \delta(t-\tau)E_{ij}$, where the information about the correlation between the noises of the

different oscillators is included in the symmetric matrix E_{ij} . In theory, the full model for the phase dynamics of a brain region oscillator should contain all the connections at once, in a single phase equation. However, due to the high dimensionality and computational expense, with equation (1) we infer a partial part of the full model dynamics related only to the two brain regions involved in a coupling connection. This procedure is then applied for each pair of brain regions.

Because of the periodic nature of the system, the coupling function can be represented by a Fourier decomposition:

$$q_{i,j}(\varphi_i, \varphi_j) = \sum_{k=-\infty}^{\infty} \sum_{s=-\infty}^{\infty} c_{i,k,s} e^{i2\pi k \varphi_i} e^{i2\pi s \varphi_j}. \quad (2)$$

For a system of two coupled oscillators, reduction to a finite number K of Fourier terms will give:

$$\dot{\varphi}_{i,j} = \sum_{k=-K}^K c_k^i \Phi_{i,j,k}(\varphi_i, \varphi_j) + \xi_i(t), \quad (3)$$

where $\Phi_{i,j,0} = 1$, $c_0^i = \omega_i$, and the rest $\Phi_{i,j,k}$ and c_k^i are the K most important Fourier components (in this work we use $K = 2$). With the assumption for a white Gaussian noise, the task is then reduced to inference of the unknown parameters of the model:

$$M = \{c_k^i, E_{ij}\}. \quad (4)$$

When the parameters of the model are inferred, one can determine then the coupling functions $q_{i,j}$ which describe the underlying mechanisms of the interaction of the oscillators³⁸.

In this work we employ the method of adaptive dynamical Bayesian inference (aDBI)^{35,36,56,57} in order to gain new insights into the oscillatory behaviour of the brain regions and the brain lobes. In this method, the time series of phases of the oscillators are considered to be time sequences of blocks of samples. In each block, the samples from a certain time interval are included, and the duration of this time interval is specified by the time window t_w . In the inference procedure, the initial assumptions for the parameters of the model are that $c_k^i = 0$, and therefore at least few inference blocks are required to obtain appropriate estimates of the model parameters values and the corresponding coupling functions. To obtain improved inference in every subsequent block, part of the information from the previous block is included in the following one. The so-called propagation parameter p_w controls how much of the information of the previous block is included in the following one. In the method of aDBI both the time window t_w and the propagation parameter p_w are adaptively determined, based on the time variabilities present in the signal. After determination of t_w and p_w the final inference is performed. This final inference provides the values of the parameters and the coupling functions for each block of inference, thus observing the time evolution of the system and the inter interactions, with a temporal resolution defined by the time window t_w . Further technical details about the parametrization, convergence and robustness of the aDBI method can be found in previous papers^{35,36,56,57}. Even though the aDBI was

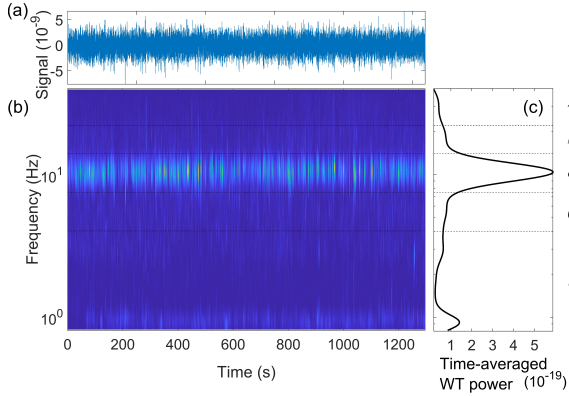


FIG. 1. Wavelet transform of the measured signal for one of the regions of one subject. The measured signal is shown in (a), while the corresponding time-frequency wavelet transform is shown in (b). The time-averaged intensity of the wavelet is shown in (c).

introduced for studies of coupled phase oscillators with oscillating frequencies in the cardiorespiratory range, the procedure is applicable to the frequency range of the brain waves as well. The application of the aDBI method on the subject dataset that was used in this study yielded a time window of $t_w = 10$ s and a propagation parameter of $p_w = 0.2$.

The aDBI method represents a further improvement of the DBI method^{35,56}, by minimizing the covariance matrix which is an indicator of the quality of the inference. The details of the method are given elsewhere³⁶ and in summary it leads to an improved inference of the model parameters without losing information about the temporal changes in the behavior of the oscillators.

B. Dataset

The dataset used in this study is publicly available⁵⁸ (<https://osf.io/mndt8/>). The data source contains the empirical region-average fMRI (functional magnetic resonance imaging), EEG source activity and structural connectomes of the 68 parcellated cortical regions of the brain of 15 healthy human subjects, age 18-31, eight of whom are female. The data consists of a resting state time series, where the subjects were asked to just stay awake and keep their eyes closed. In this study we used the empirical EEG source activity and the structural connectomes. The time series of the source activity for each patient and each cortical region have duration of 21.6 minutes with sampling frequency of 200 Hz. The description of the 68 parcellated cortical regions is given in the Appendix.

C. Wavelet transform and the phase extraction procedure

In order to check the existence of brain wave oscillations and their frequency content, the EEG time-series signals were first analyzed using a continuous wavelet transform⁵⁹⁻⁶¹. The

continuous wavelet transform is defined by the equation

$$WT(\omega, t) = \int_0^\infty \psi(\omega(u-t))x(u)\omega du, \quad (5)$$

where $x(t)$ is the signal, ω denotes the angular frequency, t is the time and

$$\psi(u) = \frac{1}{2\pi} (e^{i2\pi f_0 u} - e^{\frac{(2\pi f_0)^2}{2} u^2}) e^{-\frac{u^2}{2}}$$

is the complex Morlet wavelet, with central frequency $f_0 = 1$, $\int \psi(t) dt = 0$, and with i being the imaginary unit. The continuous wavelet transform is a time-frequency representation which contains both the phase and the amplitude dynamics of the oscillatory elements from the analyzed signal.

The initial wavelet observation of the oscillations contained in the corresponding EEG signals was carried out for several brain regions. After the initial wavelet observations, a phase extraction procedure was performed for the delta and alpha waves of the EEG signal in order to obtain the instantaneous phase time-series. These phase time-series then act as an input to the aDBI method. The oscillatory intervals were first evaluated by standard digital filtering procedure including FIR filter followed by a zero phase filtering procedure (“filtfilt”) to ensure that no time or phase lags are introduced with the filtering procedure. The delta waves signal limits were from 1 to 4 Hz, while the alpha waves signal limits were from 8 to 12 Hz⁶². The phases of the filtered signals were estimated via Hilbert transformation, thus obtaining the protophases. On these protophases, the protophase-to-phase transformation was applied⁴² in order to obtain the independent phases which act as input signals for the Bayesian inference.

D. Surrogate data testing

When oscillatory signals are analyzed, the inferred coupling between the signals is always positive and non-zero, even if the oscillators are uncoupled or unrelated. Therefore, it is necessary to establish a significance threshold in order to determine if the obtained coupling strength indicates a genuine connection and interdependence of the phenomena. Such surrogate data is used for statistical testing of the coupling strength. A threshold is usually defined by constructing randomized surrogates of the original signals^{63,64} and calculating the coupling strength for these surrogates. The coupling strength obtained in this manner represent a baseline for the confirmation of the coupling of the oscillators. In this work surrogates were constructed for each of the 68×68 delta-alpha couplings going from, and to, each of the 68 regions of the brain by using a procedure called cyclic phase permutation surrogates⁶⁴ based on rearrangement of the cycles within the extracted phase. The surrogate threshold taken in this work is the mean plus two standard deviations (mean + 2STD) of the surrogate couplings.

III. RESULTS

Fig. 1 shows the wavelet transform of the measured signal for one of the 68 brain regions in one of the subjects. The

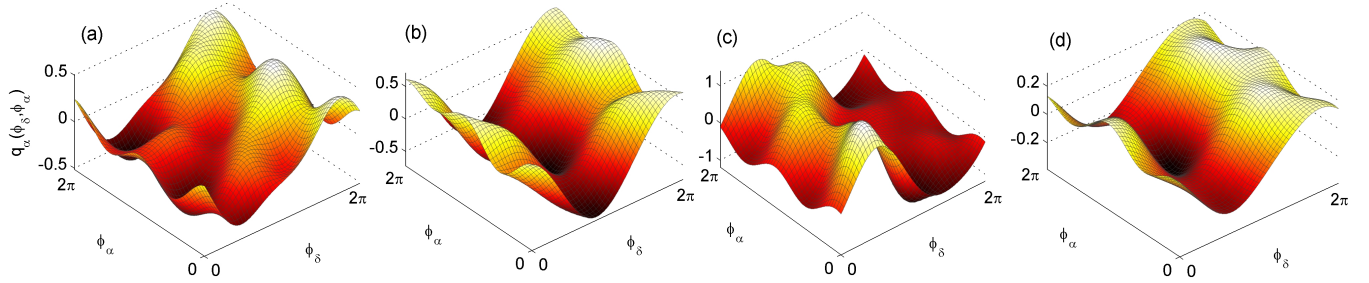


FIG. 2. The delta-alpha neural coupling functions. Examples of individual subject delta-alpha coupling functions between different regions (a)-(c). In particular, (a) shows a coupling function from subject 10 between delta region 60 and alpha region 60, (b) from subject 12 between delta region 50 and alpha region 23, and (c) from subject 6 between delta region 54 and alpha region 19. The last plot (d) shows a subject-averaged delta-alpha coupling function between delta region 58 and alpha region 21.

signal itself is presented in Fig. 1 (a), while the corresponding time-frequency wavelet transform is shown in Fig. 1 (b). To show the oscillatory frequencies present in the signal more clearly, the time-averaged intensity of the wavelet is presented in Fig. 1 (c). The frequency intervals of the corresponding brain waves are given with the dashed lines. From the figure, one can clearly see the strong alpha wave, as well as the delta wave with a slightly lower wavelet power.

The delta-alpha coupling functions are presented in Fig. 2. The coupling functions are evaluated first on individual subjects for specific regions – Fig. 2 (a)-(c). Here, they show the characteristic functional form where the delta-alpha phase coupling function depends predominately on the delta dynamics, or in other words it reflects the direct influence that the delta phase dynamics exert on the alpha phase dynamics by accelerating or decelerating the alpha brainwave oscillations. This specific form belongs to the category of direct, among the separation of self, direct and common coupling functions^{65,67}. By comparing the three plots for the coupling functions Fig. 2 (a), (b) and (c), one can notice that this direct influence is like a wave that shifts from left to right from 0 to 2π along the delta axis. In general, it keeps the direct delta dependence (i.e. it still changes predominately on delta axis) but it shifts the maximum of the function along the delta axis.

When we average the coupling functions for the same region from all the subjects, as shown in Fig. 2 (d), the remaining average delta-alpha coupling function still reflects the direct delta dependence, albeit with slightly reduced amplitude due to averaging. The Appendix A shows how this coupling function is similar or different in respect to all the order regions. Furthermore, when we average all the coupling functions across regions and subjects, the average coupling function disappeared i.e. it was insignificantly low without a common form of the function. In other words the region average coupling function averaged out, because there was no specific common form between regions.

Fig. 3 shows a 68×68 matrix representing the significant delta-alpha coupling functions for all the 68 brain regions. The vertical axis shows the number of the region for the delta brainwaves, while on the horizontal axis the number of the region of the alpha brainwaves is given. The matrix is not symmetrical and the coupling indicated by the columns is

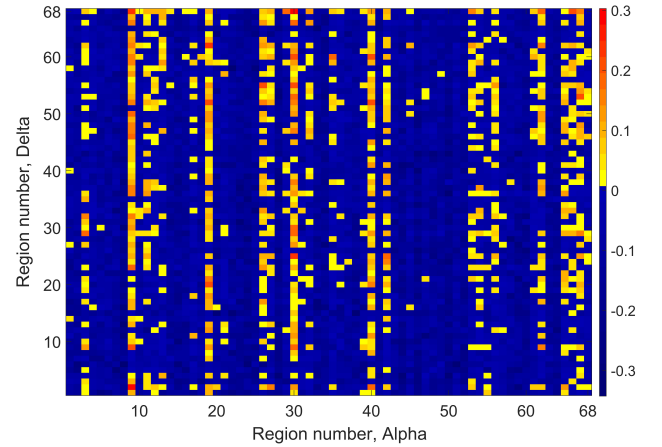


FIG. 3. Matrix 68×68 showing the delta-alpha couplings from region to region. Only those couplings which are statistically significant in respect of the surrogate threshold are shown in color (values above 0).

different than the one in the rows. The figure indicates that for some regions of the brain (e.g. columns 9, 19, 30, 40, etc) there is a stronger influence from the delta waves to the alpha waves. This is also shown in Fig. 4, where these 68 regions are marked as circles on a cross-section of the brain.

Fig. 4 (a) shows the summarized delta-alpha coupling strengths coming from a specific regions with red circles, while Fig. 4 (b) shows the sum of the delta-alpha coupling strengths for the alpha of a specific regions with blue circles. The radii of the circles are proportional to the sum of the corresponding coupling strengths. One can notice that while the significant delta-alpha couplings emanate from various different brain regions, they end up in much smaller number of the brain regions.

In order to obtain more tangible information about the overall interactions between the different brain lobes (frontal, cingulate frontal, cingulate parietal, parietal, occipital and temporal lobe), a summation of the significant coupling functions by brain lobes was performed. The sums obtained were normalized by the number of regions involved in each of the brain lobes. The results are presented in Fig. 5. The normalized

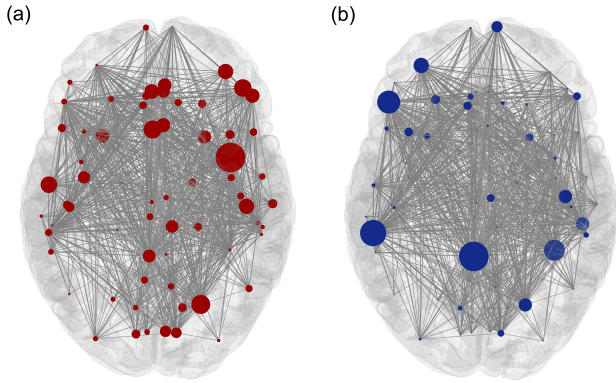


FIG. 4. Significant delta-alpha coupling strengths for the different brain regions. (a) The radii of the red circles correspond to the sum of coupling strengths of all the delta exiting the corresponding region. (b) The radii of the blue circles correspond to the sum of coupling strengths of all the alpha entering the corresponding region of the brain.

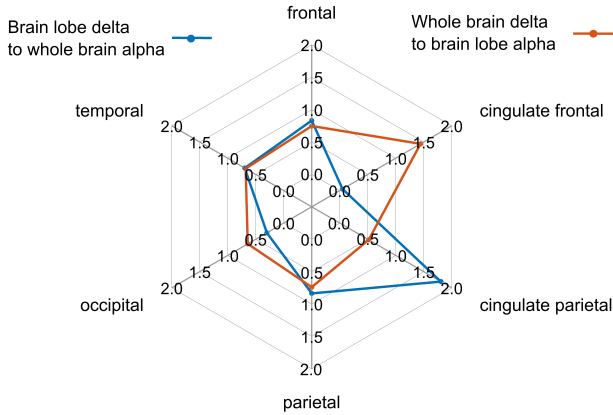


FIG. 5. Spider plot showing the influence of the separate brainwaves of the interaction into the specific brain lobes. The influence of the delta from the entire brain to the alpha of specific brain lobes (blue curve) and the influence of delta of specific brain lobes to the alpha from the entire brain (red curve).

sum of the delta-alpha couplings, where the delta is from specific brain lobe and alpha from any lobe of the brain (whole brain alpha), is shown with blue line. While the normalized sum of the delta-alpha couplings, where the delta comes from any lobe of the brain (whole brain delta) and alpha from specific brain lobe, is shown with red line. From the spider plot (Fig. 5) it can be seen that the greatest influence on the whole brain alpha has the cingulate parietal delta and at the same time the greatest influence of the whole brain delta is on the cingulate frontal alpha.

IV. DISCUSSION AND CONCLUSIONS

The influence of delta brain waves on alpha brain waves for a resting subject has previously been determined at the whole

brain level. In this paper we try to gain a deeper insight by investigating this delta-alpha influence for different brain regions according to the Desikan-Kiliany anatomical parcellation of the brain^{15,20,30,32}. As presented in the results, it can be concluded that this influence is clearly visible for different regions, because even after averaging the delta-alpha coupling functions for a particular region across all the subjects, the mean coupling function still shows the characteristic shape (Fig. 2), confirming the direct influence of the delta-phase dynamics on the alpha-phase dynamics in certain brain regions. This influence consists in acceleration or deceleration of alpha oscillations under the influence of delta oscillations.

In terms of analysis we have applied a comprehensive methodological framework for interacting brainwave oscillations. The nature of delta and alpha oscillations were observed with wavelet transform using standard parameters, with $f_0 = 1$ central frequency. This is a simple standard widely used procedure for time-frequency analysis. For the reconstruction of the phase model we used the adaptive Bayesian inference. It is a well established method which has been widely used and tested for robustness and convergence, where its parametrization has been systematically investigated on different numerical and biological systems^{35,36,56,57}. For verifying the statistical significance of the inferred delta-alpha coupling we have applied surrogate data testing⁶⁴.

The model equation (1) assumes pairwise interaction between two regions and includes only coupling function with two phase variables. This is a simplified approximation, as the brain regions form parts of a complex network, and the full model of a phase oscillator should include all the brain connections in a single equation. With equation (1) we have thus separated the inference for a partial dynamics on two-by-two basis for all the pairs of brain regions. This was possible because the Bayesian method can allow such partial dynamical filtering. While the reason to do this and separate the inference was due to the high dimensionality (68x68 regions) and the computational complexity, which otherwise could have lead to problems such as parameters overfitting. Also, we have used only pairwise coupling functions. Thus, a natural extension of this work could include also non-pairwise multivariate coupling functions^{65,66}. This is a case where the coupling function in the dynamics of one region will have more than two phase variables from phases of other regions.

The coupling function results demonstrated that there is a common waveform, predominantly due to direct influence from delta oscillations, but the wave shifts along the delta axis for different regions – Fig. 2 (a-c). We present three characteristic regions here, but the general observation from all the regions was that the wave was shifting for different regions. The quantitative analysis in Appendix A also supported this by showing relative variations of the form for different regions. The answer to why the wave for coupling function forms shifts for different regions might be because there are different lengths for the structural pathways, through which different regions interact. This most likely implies different time delays for the signal propagation^{68,69}, which is known to impact the synchronization and phase arrangement between brain regions⁷⁰ and is crucial for the information transfer⁷¹.

This time delay manifests itself as a phase shift for the oscillatory activity, i.e. $\Delta\phi$ within the phase coupling functions (e.g. as in $q_\alpha(\phi_\delta, \phi_\alpha) = \varepsilon \sin(\phi_\alpha - \phi_\delta - \Delta\phi)$), which in turn can be the cause of the phase shift of the wave observed in the figures. Our current initial observation of the structural and time delay information in this direction can stimulate future systematic analysis for quantifying how the space-time structure of the brain regions, as defined by the weights and time-delays of the connectome⁷², impacts the resulting coupling functions. Such a question is even more valid because the averaged coupling function within a region was of similar form Fig. 2 (d), while the region-averaged coupling function was averaged out. The latter implies that there is a common deterministic dependence within regions across the subjects, which is different for the separate brain regions. This kind of analysis would first require better identification of the propagation velocities and the time-delays on a personalized level, which is still not established beside promising results of MRI as a myelin biomarker⁷³, and proposed *in vivo* techniques⁶⁸. However, our results indicate that even aggregated atlases for time-delays⁶⁹ could be useful, since some of the patterns are consistent across the subjects.

We have seen that this influence is not evenly distributed across brain regions, but for certain brain regions the influence of delta oscillations on alpha oscillations is more pronounced, as is the case for isthmus cingulate, pars triangularis (associated with verbal and non-verbal communication^{74–76}) and the supramarginal region of the left hemisphere (involved in language processing^{77,78} and tool use action^{79,80}) and the fusiform region of the right hemisphere (involved in object and face recognition^{81–83}). To lesser extent this is also noticeable for the lateral orbitofrontal and the rostral middle frontal region of the left hemisphere and the inferior temporal, pars triangularis, posterior cingulate, superior parietal, frontal pole, temporal pole and transverse temporal region of the right hemisphere (see Fig.3). These regions are located in different lobes of the brain, most of them in the frontal and temporal lobes, but some in the parietal and cingulate parietal as well. No clear distinctions can be made in terms of the brain hemisphere, as is expected, since the different brain centers responsible for different actions are located in the different hemispheres.

This uneven distribution of delta influence on alpha oscillations from different regions is less pronounced on the delta side of the regions, as shown in Fig. 3 and more specifically in Fig. 4 (a). Fig. 4 shows that while the delta-alpha influence is more concentrated for the alpha waves in certain regions, the distributions of significant couplings in terms of delta waves is more even across brain regions. This means that the influencing oscillations are more evenly distributed across the brain regions than the influenced oscillations, which are more concentrated in certain regions.

Additional insights into delta-alpha influences in the brain can be gained by condensing this information down to the level of brain lobes, as shown in the spider plot (Fig. 5). These results indicate that the influence of delta oscillations of all brain regions is greatest on alpha oscillations of the cingulate frontal lobe. At the same time, the influence of cingulate pari-

etal brain lobe's delta oscillations on the alpha oscillations is greatest among all the regions of the brain. This influence of the cingulate frontal and cingulate parietal regions of the brain on other brain regions and on the brain as a whole should be further investigated and put into the context of the functioning of the brain from a neurological point of view.

Finally, it is worth noting that we presented the methodological framework for interactions in the brain regions network for the resting state, however, the framework carries important implications and can readily be used also for other neural states, or interacting oscillatory networks more generally.

ACKNOWLEDGMENTS

D.L., T.S. and P.J. acknowledge support from the bilateral Macedonian - Chinese project for scientific and technological cooperation. P.J. acknowledge support from STI2030-Major Projects (2021ZD0204500), the NSFC (62076071), and Shanghai Municipal Science and Technology Major Project (2018SHZDZX01).

DATA AVAILABILITY STATEMENT

The data that support the findings of this study are publicly available.

V. REFERENCES

- ¹H.-J. Park and K. Friston, "Structural and functional brain networks: from connections to cognition," *Science* **342**, 1238411 (2013).
- ²K. Lehnertz, G. Ansmann, S. Bialonski, H. Dickten, C. Geier, and S. Porz, "Evolving networks in the human epileptic brain," *Physica D* **267**, 7–15 (2014).
- ³L. R. Chai, A. N. Khambhati, R. Ciric, T. M. Moore, R. C. Gur, R. E. Gur, T. D. Satterthwaite, and D. S. Bassett, "Evolution of brain network dynamics in neurodevelopment," *Network Neuroscience* **1**, 14–30 (2017).
- ⁴D. Rudrauf, A. Douiri, C. Kovach, J. P. Lachaux, D. Cosmelli, M. Chavez, C. Adam, B. Renault, J. Martinerie, and M. L. Van Quyen, "Frequency flows and the time-frequency dynamics of multivariate phase synchronization in brain signals," *NeuroImage* **31**, 209–227 (2006).
- ⁵Q. Li, T. Peron, T. Stankovski, and P. Ji, "Effects of structural modifications on cluster synchronization patterns," *Nonlinear Dynamics* **108**, 3529–3541 (2022).
- ⁶P. Sauseng, W. Klimesch, W. R. Gruber, and N. Birbaumer, "Cross-frequency phase synchronization: a brain mechanism of memory matching and attention," *Neuroimage* **40**, 308–317 (2008).
- ⁷X. Suo, D. Lei, K. Li, F. Chen, F. Li, L. Li, X. Huang, S. Lui, L. Li, G. J. Kemp, *et al.*, "Disrupted brain network topology in pediatric posttraumatic stress disorder: A resting-state fmri study," *Human brain mapping* **36**, 3677–3686 (2015).
- ⁸K. T. Olde Dubbelink, A. Hillebrand, D. Stoffers, J. B. Deijen, J. W. Twisk, C. J. Stam, and H. W. Berendse, "Disrupted brain network topology in parkinson's disease: a longitudinal magnetoencephalography study," *Brain* **137**, 197–207 (2014).
- ⁹R. S. Desikan, F. Ségonne, B. Fischl, B. T. Quinn, B. C. Dickerson, D. Blacker, R. L. Buckner, A. M. Dale, R. P. Maguire, B. T. Hyman, M. S. Albert, and R. J. Killiany, "An automated labeling system for subdividing the human cerebral cortex on mri scans into gyral based regions of interest," *NeuroImage* **31**, 968–980 (2006).

- ¹⁰L. Fan, H. Li, J. Zhuo, Y. Zhang, J. Wang, L. Chen, Z. Yang, C. Chu, S. Xie, A. R. Laird, *et al.*, “The human brainnetome atlas: a new brain atlas based on connective architecture,” *Cerebral cortex* **26**, 3508–3526 (2016).
- ¹¹M. F. Glasser, T. S. Coalson, E. C. Robinson, C. D. Hacker, J. Harwell, E. Yacoub, K. Ugurbil, J. Andersson, C. F. Beckmann, M. Jenkinson, *et al.*, “A multi-modal parcellation of human cerebral cortex,” *Nature* **536**, 171–178 (2016).
- ¹²R. T. Canolty, E. Edwards, S. S. Dalal, M. Soltani, S. S. Nagarajan, H. E. Kirsch, M. S. Berger, N. M. Barbaro, and R. T. Knight, “High gamma power is phase-locked to theta oscillations in human neocortex,” *Science* **313**, 1626–1628 (2006).
- ¹³O. Jensen and L. L. Colgin, “Cross-frequency coupling between neuronal oscillations,” *Trends Cognit. Sci.* **11**, 267–269 (2007).
- ¹⁴J. M. Palva, S. Palva, and K. Kaila, “Phase synchrony among neuronal oscillations in the human cortex,” *J. Neurosci.* **25**, 3962–3972 (2005).
- ¹⁵V. Jirsa and V. Müller, “Cross-frequency coupling in real and virtual brain networks,” *Frontiers Comput. Neurosci.* **7**, 78 (2013).
- ¹⁶P. Sorrentino, M. Ambrosiano, R. Rucco, J. Cabral, L. L. Gollo, M. Breakspear, and F. Baseliace, “Detection of cross-frequency coupling between brain areas: An extension of phase linearity measurement,” *Frontiers in Neuroscience* **16** (2022).
- ¹⁷M. K. Delimayanti, B. Purnama, N. G. Nguyen, M. R. Faisal, K. R. Mahmudah, F. Indriani, M. Kubo, and K. Satou, “Classification of brainwaves for sleep stages by high-dimensional fft features from eeg signals,” *Applied Sciences* **10**, 1797 (2020).
- ¹⁸M. Gorgoni, S. Scarpelli, F. Reda, and L. De Gennaro, “Sleep eeg oscillations in neurodevelopmental disorders without intellectual disabilities,” *Sleep Medicine Reviews* **49**, 101224 (2020).
- ¹⁹J. M. Krueger, M. G. Frank, J. P. Wisor, and S. Roy, “Sleep function: Toward elucidating an enigma,” *Sleep medicine reviews* **28**, 46–54 (2016).
- ²⁰A. Bashan, R. P. Bartsch, J. W. Kantelhardt, S. Havlin, and P. C. Ivanov, “Network physiology reveals relations between network topology and physiological function,” *Nat. Commun.* **3**, 702 (2012).
- ²¹T. Penzel, M. Hirshkowitz, J. Harsh, R. D. Chervin, N. Butkov 5, M. Kryger, B. Malow, M. V. Vitiello, M. H. Silber, C. A. Kushida, *et al.*, “Digital analysis and technical specifications,” *Journal of clinical sleep medicine* **3**, 109–120 (2007).
- ²²S. Palva and J. M. Palva, “New vistas for α -frequency band oscillations,” *Trends Neurosci.* **30**, 150–158 (2007).
- ²³C. L. Ehlers and D. J. Kupfer, “Effects of age on delta and rem sleep parameters,” *Electroencephalography and clinical neurophysiology* **72**, 118–125 (1989).
- ²⁴M. S. Keshavan, C. F. Reynolds, J. M. Miewald, D. M. Montrose, J. A. Sweeney, R. C. Vasko, and D. J. Kupfer, “Delta sleep deficits in schizophrenia: evidence from automated analyses of sleep data,” *Archives of general psychiatry* **55**, 443–448 (1998).
- ²⁵R. M. Benca, W. H. Obermeyer, C. L. Larson, B. Yun, I. Dolski, K. D. Kleist, S. M. Weber, and R. J. Davidson, “Eeg alpha power and alpha power asymmetry in sleep and wakefulness,” *Psychophysiology* **36**, 430–436 (1999).
- ²⁶W. Scheuler, D. Stinshoff, and S. Kubicki, “The alpha-sleep pattern,” *Neuropsychobiology* **10**, 183–189 (1983).
- ²⁷P. Hauri and D. R. Hawkins, “Alpha-delta sleep,” *Electroencephalography and clinical Neurophysiology* **34**, 233–237 (1973).
- ²⁸S. Vijayan, E. B. Klerman, G. K. Adler, and N. J. Kopell, “Thalamic mechanisms underlying alpha-delta sleep with implications for fibromyalgia,” *Journal of neurophysiology* **114**, 1923–1930 (2015).
- ²⁹T. Stankovski, S. Petkoski, J. Raeder, A. F. Smith, P. V. E. McClintock, and A. Stefanovska, “Alterations in the coupling functions between cortical and cardio-respiratory oscillations due to anaesthesia with propofol and sevoflurane,” *Phil. Trans. R. Soc. A* **374**, 20150186 (2016).
- ³⁰T. Stankovski, V. Ticcinielli, P. V. E. McClintock, and A. Stefanovska, “Neural cross-frequency coupling functions,” *Front. Syst. Neurosci.* **11**, 10.3389/fnsys.2017.00033 (2017).
- ³¹Manasova, D. & Stankovski, T. Neural Cross-Frequency Coupling Functions in Sleep. *Neuroscience*. **523** pp. 20-30 (2023)
- ³²J. R. Isler, P. G. Grieve, D. Czernochowski, R. I. Stark, and D. Friedman, “Cross-frequency phase coupling of brain rhythms during the orienting response,” *Brain Res.* **1232**, 163–172 (2008).
- ³³Y. Kuramoto, *Chemical Oscillations, Waves, and Turbulence* (Springer-Verlag, Berlin, 1984).
- ³⁴V. N. Smelyanskiy, D. G. Luchinsky, A. Stefanovska, and P. V. E. McClintock, “Inference of a nonlinear stochastic model of the cardiorespiratory interaction,” *Phys. Rev. Lett.* **94**, 098101 (2005).
- ³⁵T. Stankovski, A. Duggento, P. V. E. McClintock, and A. Stefanovska, “Inference of time-evolving coupled dynamical systems in the presence of noise,” *Phys. Rev. Lett.* **109**, 024101 (2012).
- ³⁶D. Lukarski, M. Ginovska, H. Spasevska, and T. Stankovski, “Time window determination for inference of time-varying dynamics: application to cardiorespiratory interaction,” *Frontiers in Physiology* **11** (2020).
- ³⁷K. J. Friston, “Functional and effective connectivity: a review,” *Brain. Connect.* **1**, 13–36 (2011).
- ³⁸T. Stankovski, T. Pereira, P. V. E. McClintock, and A. Stefanovska, “Coupling functions: Universal insights into dynamical interaction mechanisms,” *Rev. Mod. Phys.* **89**, 045001 (2017).
- ³⁹I. Z. Kiss, C. G. Rusin, H. Kori, and J. L. Hudson, “Engineering complex dynamical structures: Sequential patterns and desynchronization,” *Science* **316**, 1886–1889 (2007).
- ⁴⁰W. Moon and J. S. Wettlaufer, “Coupling functions in climate,” *Philosophical Transactions of the Royal Society A* **377**, 20190006 (2019).
- ⁴¹T. Stankovski, P. V. E. McClintock, and A. Stefanovska, “Coupling functions enable secure communications,” *Phys. Rev. X* **4**, 011026 (2014).
- ⁴²B. Kraleman, L. Cimponeriu, M. Rosenblum, A. Pikovsky, and R. Mrowka, “Phase dynamics of coupled oscillators reconstructed from data,” *Phys. Rev. E* **77**, 066205 (2008).
- ⁴³S. Ranganathan, V. Spaiser, R. P. Mann, and D. J. T. Sumpter, “Bayesian dynamical systems modelling in the social sciences,” *PLoS ONE* **9**, e86468 (2014).
- ⁴⁴B. Kraleman, M. Frühwirth, A. Pikovsky, M. Rosenblum, T. Kenner, J. Schaefer, and M. Moser, “In vivo cardiac phase response curve elucidates human respiratory heart rate variability,” *Nat. Commun.* **4**, 2418 (2013).
- ⁴⁵D. Lukarski, D. Stavrov, and T. Stankovski, “Variability of cardiorespiratory interactions under different breathing patterns,” *Biomedical Signal Processing and Control* **71**, 103152 (2022).
- ⁴⁶T. Stankovski, “Coupling functions in neuroscience,” in *Physics of Biological Oscillators* (Springer, 2021) pp. 175–189.
- ⁴⁷C. Bick, M. Goodfellow, C. R. Laing, and E. A. Martens, “Understanding the dynamics of biological and neural oscillator networks through exact mean-field reductions: a review,” *Journal of Mathematical Neuroscience* **10**, 9 (2020).
- ⁴⁸A. Yeldesbay, G. R. Fink, and S. Daun, “Reconstruction of effective connectivity in the case of asymmetric phase distributions,” *Journal of neuroscience methods* (2019).
- ⁴⁹K. Suzuki, T. Aoyagi, and K. Kitano, “Bayesian estimation of phase dynamics based on partially sampled spikes generated by realistic model neurons,” *Frontiers in computational neuroscience* **11**, 116 (2018).
- ⁵⁰A. Jafarian, P. Zeidman, V. Litvak, and K. Friston, “Structure learning in coupled dynamical systems and dynamic causal modelling,” *Phil. Trans. R. Soc. A* **377**, 20190048 (2019).
- ⁵¹H. Su, C. Huo, B. Wang, W. Li, G. Xu, Q. Liu, and Z. Li, “Alterations in the coupling functions between cerebral oxyhaemoglobin and arterial blood pressure signals in post-stroke subjects,” *PLoS one* **13**, e0195936 (2018).
- ⁵²C. N. Takembo, A. Mvogo, H. P. E. Fouda, and T. C. Kofané, “Effect of electromagnetic radiation on the dynamics of spatiotemporal patterns in memristor-based neuronal network,” *Nonlinear Dynamics*, 1–12 (2018).
- ⁵³A. Gruszecka, M. K. Nuckowska, M. Waskow, J. Kot, P. J. Winklewski, W. Guminski, A. F. Frydrychowski, J. Wtorek, A. Bujnowski, P. Lass, *et al.*, “Coupling between blood pressure and subarachnoid space width oscillations during slow breathing,” *Entropy* **23**, 113 (2021).
- ⁵⁴H. Nakao, T. Yanagita, and Y. Kawamura, “Phase-reduction approach to synchronization of spatiotemporal rhythms in reaction-diffusion systems,” *Phys. Rev. X* **4**, 021032 (2014).
- ⁵⁵F. A. Rodrigues, T. K. D. M. Peron, P. Ji, and J. Kurths, “The Kuramoto model in complex networks,” *Phys. Rep.* **610**, 1–98 (2016).
- ⁵⁶A. Duggento, T. Stankovski, P. V. E. McClintock, and A. Stefanovska, “Dynamical Bayesian inference of time-evolving interactions: From a pair of coupled oscillators to networks of oscillators,” *Phys. Rev. E* **86**, 061126 (2012).

- ⁵⁷T. Stankovski, A. Duggento, P. V. E. McClintock, and A. Stefanovska, "A tutorial on time-evolving dynamical Bayesian inference," *Eur. Phys. J. Special Topics* **223**, 2685–2703 (2014).
- ⁵⁸M. Schirner, A. R. McIntosh, V. Jirsa, G. Deco, and P. Ritter, "Inferring multi-scale neural mechanisms with brain network modelling," *eLife* **7**, e28927 (2018).
- ⁵⁹I. Daubechies, *Ten lectures on wavelets* (SIAM, 1992).
- ⁶⁰G. Kaiser, *A Friendly Guide to Wavelets* (Birkhäuser, Boston, 1994).
- ⁶¹A. Stefanovska, M. Bračić, and H. D. Kvernmo, "Wavelet analysis of oscillations in the peripheral blood circulation measured by laser Doppler technique," *IEEE Trans. Bio. Med. Eng.* **46**, 1230–1239 (1999).
- ⁶²G. Buzsáki and A. Draguhn, "Neuronal oscillations in cortical networks," *Science* **304**, 1926–1929 (2004).
- ⁶³T. Schreiber and A. Schmitz, "Surrogate time series," *Physica D* **142**, 346–382 (2000).
- ⁶⁴G. Lancaster, D. Iatsenko, A. Pidde, V. Ticcinelli, and A. Stefanovska, "Surrogate data for hypothesis testing of physical systems," *Phys. Rep.* **748**, 1–60 (2018).
- ⁶⁵T. Stankovski, V. Ticcinelli, P. V. E. McClintock, and A. Stefanovska, "Coupling functions in networks of oscillators," *New J. Phys.* **17**, 035002 (2015).
- ⁶⁶F. Battiston, G. Cencetti, I. Iacopini, V. Latora, M. Lucas, A. Patania, J. Young, and G. Petri, "Networks beyond pairwise interactions: Structure and dynamics," *Phys. Rep.* **874**, 1–92 (2020).
- ⁶⁷D. Iatsenko, A. Bernjak, T. Stankovski, Y. Shiozai, P. J. Owen-Lynch, P. B. M. Clarkson, P. V. E. McClintock, and A. Stefanovska, "Evolution of cardio-respiratory interactions with age," *Phil. Trans. R. Soc. Lond. A* **371**, 20110622 (2013).
- ⁶⁸P. Sorrentino, S. Petkoski, M. Sparaco, E. T. Lopez, R. Rucco, E. Signoriello, F. Baselice, S. Bonavita, M. Pirozzi, M. Quarantelli, G. Sorrentino, and V. Jirsa, "Whole-brain propagation delays in multiple sclerosis, a combined tractography - magnetoencephalography study," *Journal of Neuroscience*, JN–RM–0938–22 (2022).
- ⁶⁹J.-D. Lemaréchal, M. Jedynak, L. Trebaul, A. Boyer, F. Tadel, M. Bhat-tacharjee, P. Deman, V. Tuyisenge, L. Ayoubian, E. Hugues, *et al.*, "A brain atlas of axonal and synaptic delays based on modelling of cortico-cortical evoked potentials," *Brain-A Journal of Neurology* (2021).
- ⁷⁰S. Petkoski and V. K. Jirsa, "Transmission time delays organize the brain network synchronization," *Philosophical Transactions of the Royal Society A: Mathematical, Physical and Engineering Sciences* **377**, 20180132 (2019).
- ⁷¹P. Fries, "Rhythms for Cognition: Communication through Coherence," *Neuron* **88**, 220–235 (2015).
- ⁷²S. Petkoski and V. K. Jirsa, "Normalizing the brain connectome for communication through synchronization," *Network Neuroscience* **6**, 722–744 (2022).
- ⁷³M. Mancini, A. Karakuzu, J. Cohen-Adad, M. Cercignani, T. E. Nichols, and N. Stikov, "An interactive meta-analysis of mri biomarkers of myelin," *Elife* **9**, e61523 (2020).
- ⁷⁴A. L. Foundas, C. M. Leonard, R. L. Gilmore, E. B. Fennell, and K. M. Heilman, "Pars triangularis asymmetry and language dominance," *Proceedings of the National Academy of Sciences of the United States of America* **93**, 719–722 (1996).
- ⁷⁵J. Mai and G. Paxinos, *The Human Nervous System* (Elsevier Science, 2011).
- ⁷⁶P. Johns, *Clinical Neuroscience: An Illustrated Colour Text*, An Illustrated Colour Text Series (Churchill Livingstone/Elsevier, 2014).
- ⁷⁷I. Deschamps, S. R. Baum, and V. L. Gracco, "On the role of the supra-marginal gyrus in phonological processing and verbal working memory: Evidence from rTMS studies," *Neuropsychologia* **53**, 39–46 (2014).
- ⁷⁸J. Leinweber, S. Heim, F. Altenbach, A. Chatterjee, U. Habel, and K. Sass, "Deeper insights into semantic relations: An fmri study of part-whole and functional associations," *Brain and language* **129C**, 30–42 (2014).
- ⁷⁹L. Ma, S. Narayana, D. Robin, P. Fox, and J. Xiong, "Changes occur in resting state network of motor system during 4 weeks of motor skill learning," *NeuroImage* **58**, 226–33 (2011).
- ⁸⁰A. Assmus, J. Marshall, A. Ritzl, J. Noth, K. Zilles, and G. Fink, "Left inferior parietal cortex integrates time and space during collision judgments," *NeuroImage* **20 Suppl 1**, S82–8 (2003).
- ⁸¹Y. Zhao, Z. Zhen, X. Liu, Y. Song, and J. Liu, "The neural network for face recognition: Insights from an fmri study on developmental prosopagnosia,"

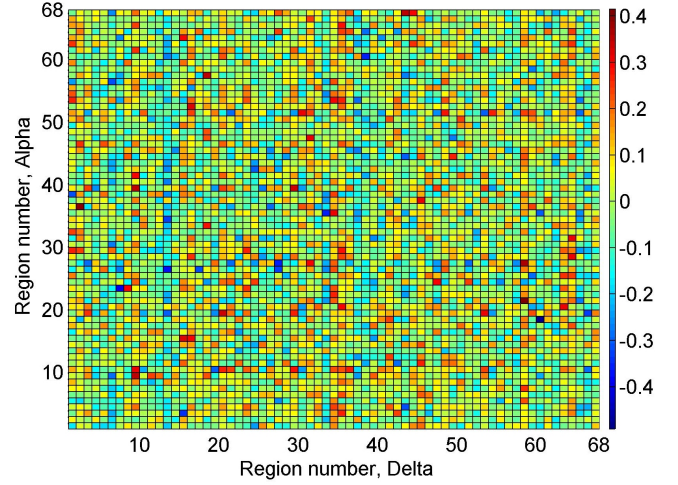


FIG. 6. Matrix 68×68 showing the similarity index for different regions of the brain. The similarity index shows the average similarity for the 15 subjects between the coupling function for a particular brain region and the average coupling function for all subjects between delta region 58 and alpha region 21.

- NeuroImage* **169**, 151–161 (2018).
- ⁸²K. Katanoda, K. Yoshikawa, and M. Sugishita, "Neural substrates for the recognition of newly learned faces: a functional mri study," *Neuropsychologia* **38**, 1616–1625 (2000).
- ⁸³V. Axelrod and G. Yovel, "Successful decoding of famous faces in the fusiform face area," *PloS one* **10**, e0117126 (2015).

Appendix A: Similarity index for the inferred coupling functions

The analysis about the coupling functions in Fig. 2 shows qualitatively that there is a similar form for different regions for some subjects and for subject average on some regions. To quantify how big is this similarity and how much there is variations and differences from the coupling functions presented, now we calculate the similarity in respect to all the other regions.

One way to quantify the form of the coupling functions is to use the so-called similarity index⁴⁴ between the coupling functions. The similarity index measure, ρ , gives the similarity between two coupling functions q_1 and q_2 , regardless of their coupling strengths. Thus, the similarity index ρ is a coupling function unique measure that quantifies the form of the functions. It is calculated as correlation between the coefficients from the inferred coupling parameters⁴⁴. The index is determined as:

$$\rho = \frac{\langle \tilde{q}_1 \tilde{q}_2 \rangle}{\|\tilde{q}_1\| \|\tilde{q}_2\|} \quad (\text{A1})$$

where $\langle q \rangle$ denotes spatial averaging over a two dimensional domain $0 \leq \varphi_1, \varphi_2 \leq 2\pi$, and $\tilde{q} = q - \langle q \rangle$ and $\|q\| = \langle qq \rangle^{1/2}$.

The results for the similarity index ρ for the inferred coupling functions across regions are shown in Fig. 6. The indices

presented show the average similarity for all the subjects between the coupling functions of each region and the average coupling function for all subjects for a characteristic case between delta region 58 and alpha region 21 i.e. the coupling function as presented in Fig. 2 (d). Or in other words, because we could not present visually all the $68 \times 68 = 4624$ coupling function combinations, in the main text we present some characteristic cases, and here in the Appendix with Fig. 6 we extend this by quantitative analysis with all the other cases. Thus, Fig. 6 shows the extent of similarity and deviations from the visually presented coupling functions. From the observations, one can notice that there are relative variations of the form, with some regions being more or less similar, and there is also negative similarity i.e. π -shifted similarity.

Appendix B: Sample size robustness – variance of the coupling functions in respect to number of subjects

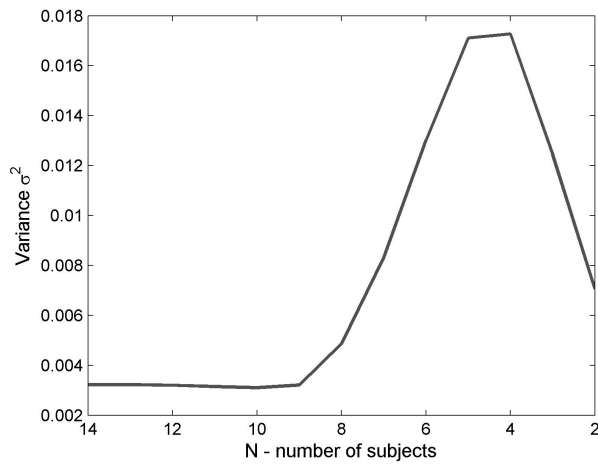


FIG. 7. Sample-size effect on the subject-averaged delta-alpha coupling function. The plot shows dependence of the variance in respect to the number N of subjects averaged. The variance is calculated from the similarity index between the full ($N=15$) subject averaged coupling function and the coupling functions from all the combinations of lower N number of subjects. All the coupling functions are for delta region 58 and alpha region 21.

The coupling function analysis were perform on sample of $N=15$ subjects. In order to test if the number of subjects had an effect on the resulting average coupling function (like e.g. in Fig. 2(d)) we tested how much the coupling function varies when smaller number of subjects is averaged. This was done by systematically calculating the average coupling function from smaller number of subjects $N=14$, then $N=13$, and so on until $N=2$. Here, for each smaller N we calculated the average coupling function for all N -combinations. Then, we calculated the similarity index ρ between each N average coupling function and the coupling function from all 15 subjects (as in Fig. 2(d)). Finally, we calculated the variance for all similarity indexes of each combination for one N . For example for $N=14$, there are 15 different combinations of $N=14$ subject groups; we calculated 15 average coupling functions and compared the similarity index of each in respect of the full coupling function, so as to calculate the variance of this 15 ρ indexes.

Fig. 7 shows the variance dependence on the reduced number of subjects N . One can notice that the variance is relatively low. The dependence on N shows that the variance is low for reducing N until $N=10$ (perhaps $N=9$), after which for lower N the variance is rapidly increased. Therefore, the full number of sample size $N=15$ subjects is quite robust and has no big effect on the averaged coupling function. The results in Fig. 7 were calculated for two regions (delta 58 and alpha 21), but our investigation on other regions showed similar results for the variance where it was low for $N=10$ and then it got rapidly increased.

Appendix C: Association of region numbers to appropriate brain regions

Table I shows the relationship between the ordinal numbers of the regions as used in this paper and the designations of the regions according to the Desikan-Kiliany anatomical parcellation.

TABLE I. Relationship between the ordinal numbers of the regions as used in this paper and the designations of the regions according to the Desikan-Kiliany anatomical parcellation.

Region number	Brain region	Hemisphere	Brain lobe	Region number	Brain region	Hemisphere	Brain lobe
1	banksst	left	temporal	35	banksst	right	temporal
2	caudalanteriorcingulate	left	cingulate frontal	36	caudalanteriorcingulate	right	cingulate frontal
3	caudalmiddlefrontal	left	frontal	37	caudalmiddlefrontal	right	frontal
4	cuneus	left	occipital	38	cuneus	right	occipital
5	entorhinal	left	temporal	39	entorhinal	right	temporal
6	fusiform	left	temporal	40	fusiform	right	temporal
7	inferiorparietal	left	parietal	41	inferiorparietal	right	parietal
8	inferiortemporal	left	temporal	42	inferiortemporal	right	temporal
9	isthmuscingulate	left	cingulate parietal	43	isthmuscingulate	right	cingulate parietal
10	lateraloccipital	left	occipital	44	lateraloccipital	right	occipital
11	lateralorbitofrontal	left	frontal	45	lateralorbitofrontal	right	frontal
12	lingual	left	occipital	46	lingual	right	occipital
13	medialorbitofrontal	left	frontal	47	medialorbitofrontal	right	frontal
14	middletemporal	left	temporal	48	middletemporal	right	temporal
15	parahippocampal	left	temporal	49	parahippocampal	right	temporal
16	paracentral	left	frontal	50	paracentral	right	frontal
17	parsopercularis	left	frontal	51	parsopercularis	right	frontal
18	parsorbitalis	left	frontal	52	parsorbitalis	right	frontal
19	parstriangularis	left	frontal	53	parstriangularis	right	frontal
20	pericalcarine	left	occipital	54	pericalcarine	right	occipital
21	postcentral	left	parietal	55	postcentral	right	parietal
22	posteriorcingulate	left	cingulate parietal	56	posteriorcingulate	right	cingulate parietal
23	precentral	left	frontal	57	precentral	right	frontal
24	precuneus	left	parietal	58	precuneus	right	parietal
25	rostralanteriorcingulate	left	cingulate frontal	59	rostralanteriorcingulate	right	cingulate frontal
26	rostralmiddlefrontal	left	frontal	60	rostralmiddlefrontal	right	frontal
27	superiorfrontal	left	frontal	61	superiorfrontal	right	frontal
28	superiorparietal	left	parietal	62	superiorparietal	right	parietal
29	superiortemporal	left	temporal	63	superiortemporal	right	temporal
30	supramarginal	left	parietal	64	supramarginal	right	parietal
31	frontalpole	left	frontal	65	frontalpole	right	frontal
32	temporalpole	left	temporal	66	temporalpole	right	temporal
33	transversetemporal	left	temporal	67	transversetemporal	right	temporal
34	insula	left	temporal	68	insula	right	temporal